◆ Human Brain Mapping 37:819–832 (2016) ◆

Atypical Age-Dependent Effects of Autism on White Matter Microstructure in Children of 2–7 Years

Minhui Ouyang,[1,2,3] Hua Cheng,[4] Virendra Mishra,[2] Gaolang Gong,[5] Matthew W. Mosconi,[6,7] John Sweeney,[6,7] Yun Peng,[4] and Hao Huang[1,2,8]*

[1]Department of Radiolog , Children's Hospital of Philadelphia, Penns lvania
[2]Advanced Imaging Research Center, Universit of Texas Southwestern Medical Center, Texas
[3]Biomedical Engineering Joint Graduate Program, Universit of Texas at Arlington-Universit of Texas Southwestern Medical Center, Texas
[4]Department of Radiolog , Beijing Children's Hospital, Capital Medical Universit , Beijing, China
[5]State Ke Laborator of Cognitive Neuroscience and Learning, Beijing Normal Universit , Beijing, China
[6]Center for Autism and Developmental Disabilities, Universit of Texas Southwestern Medical Center, Dallas, Texas
[7]Department of Ps chiatr , Universit of Texas Southwestern Medical Center, Dallas, Texas
[8]Department of Radiolog , Perelman School of Medicine, Universit of Penns lvania, Penns lvania

Abstract: Atypical age-dependent changes of white matter (WM) microstructure play a central role in abnormal brain maturation of the children with autism spectrum disorder (ASD), but their early manifestations have not been systematically characterized. The entire brain core WM voxels were surveyed to detect differences in WM microstructural development between 31 children with ASD of 2–7 years and 19 age-matched children with typical development (TD), using measurements of fractional anisotropy (FA) and radial diffusivity (RD) from diffusion tensor imaging (DTI). The anatomical locations, distribution, and extent of the core WM voxels with atypical age-dependent changes in a specific tract or tract group were delineated and evaluated by integrating the skeletonized WM with a digital atlas. Exclusively, unidirectional FA increases and RD decreases in widespread WM tracts were revealed in children with ASD before 4 years, with bi-directional changes found for children with ASD of 2–7 years. Compared to progressive development that raised FA and lowered RD during 2–7 years in the TD group, flattened curves of WM maturation were found in multiple major WM tracts of all five tract groups, particularly associational and limbic tracts, in the ASD group with trend lines of ASD and TD crossed around 4 years. We found atypical age-dependent changes of FA and RD widely and heterogeneously distributed in WM tracts of children with ASD. The early higher WM microstructural integrity before 4 years reflects abnormal neural patterning, connectivity, and pruning that may

Additional Supporting Information may be found in the online version of this article.

Contract grant sponsor: NIH; Contract grant numbers: MH092535 and MH092535-S1, HH

*Correspondence to: Hao Huang, 34th street and Civic Center blvd, Philadelphia, PA 19104. E-mail: huangh6@email.chop.edu

Received for publication 6 August 2015; Accepted 22 November 2015.

DOI: 10.1002/hbm.23073
Published online 10 December 2015 in Wiley Online Library (wileyonlinelibrary.com).

contribute to aberrant behavioral and cognitive development in ASD. *Hum Brain Mapp 37:819 832, 2016.*

Key words: autism; children; atypical; microstructure; white matter; development

INTRODUCTION

Autism spectrum disorder (ASD) is a neurodevelopmental disorder with multiple causes [Penagarikano et al., 2011; Zhao et al., 2007]. It is behaviorally defined based on impairments in communication and social interactions, repetitive and ritualized behaviors, and restricted interests [APA, 2000; Kanner, 1968]. The diagnosis of ASD often can be reliably determined by age 2 years [Baird et al., 2003], although the mean age at which children are initially diagnosed is frequently higher (range 38–120 months) [Daniels and Mandell, 2013]. Identifying atypical brain white matter (WM) processes in early childhood is critical to understanding the neurobiology of the disorder and may be informative for identifying the disorder earlier in its course.

Diffusion tensor imaging (DTI), one type of magnetic resonance imaging (MRI) capable of delineating macroscopic WM tract pathways and detecting WM microstructural pathology by measuring water diffusion in the brain [Basser et al., 1994], may be particularly useful for identifying early emerging WM neurodevelopmental alterations in ASD. The directional dependence of water diffusion preferentially along the axis of an axonal bundle makes noninvasive tracing of WM tracts possible with DTI tractography [Mori et al., 1999; Wakana et al., 2007]. Fractional anisotropy (FA), one of the most widely used DTI derived metrics, characterizes the shape of the diffusion tensor and is sensitive to WM microstructural disruption [Beaulieu, 2002]. Radial diffusivity (RD), quantifying the magnitude of diffusion orthogonal to the principal diffusion direction, is believed to reflect the extent of WM myelination [Song et al., 2005]. The WM anatomy can be delineated with a digital WM atlas and parcellated into 48 major WM tracts [Mori et al., 2008]. These WM tracts are categorized into five functionally distinguished tract groups [Huang et al., 2012a; Wakana et al., 2004], namely commissural (right-left hemispheric connections), association (cortex–cortex connections), limbic (connectivity in the limbic system), projection (cortex–spinal cord, cortex–thalamus connections), and brainstem (including brain stem and cerebellar WM) tract groups.

The majority of DTI studies investigating ASD have focused on the age range from mid-childhood and adolescence to adulthood [e.g. Barnea-Goraly et al., 2005; Travers et al., 2012] when the clinical manifestations have well emerged [Paus et al., 2008]. These studies demonstrated decreased FA, increased mean diffusivity (MD), and increased RD in individuals with ASD compared to those with typical development (TD). DTI studies of children with ASD less than 10 years of age are relatively rare and results were not uniform, suggesting variable age-related effects in ASD. For example, strengthened WM integrity with increased FA has been reported for various WM regions in ASD children of 1.8–3.3 years [Ben Bashat et al., 2007], 1.5–5.8 years [Weinstein et al., 2011], and 0.5–2 years [Wolff et al., 2012]. In contrast, reduced WM integrity with lower FA and higher MD has also been found in various WM regions in slightly older children with ASD of 4.79 ± 2.43 years [Sundaram et al., 2008], 2.5–8.9 years [Kumar et al., 2010], and 2–8 years [Walker et al., 2012]. Thus, WM microstructural changes of ASD are both region- and age-dependent, especially in early development.

Early years of life including 2–7 years mark an important period for the formation of neural wiring patterns [Casey et al., 2005]. This period is critical for brain development and early intervention [Courchesne et al., 2007; Sowell and Bookheimer, 2012]. To date, there has been no analysis of WM based on parcellated tract or tract group for children with ASD of age 2–7 years. There was no further quantification of the extent of atypical WM development in any specific tract or tract group in individuals with ASD across early childhood (ages 2–7 years), either. The study of Walker et al. [Walker et al., 2012] has examined whole brain WM. However, without integration of the parcellated tract [Mori et al., 2008], only abnormality of limited large tracts (e.g. corpus callosum), instead of all major 48 WM tracts, was qualitatively characterized. With WM tracts underlying structural connectivity among different brain regions, systematically quantifying the age-dependent effects of ASD on WM microstructural changes with individual tract as a reference has significance for understanding heterogeneous clinical manifestations related to different WM tract function and furthermore early brain developmental mechanisms associated with ASD.

In this study, we hypothesized that children with ASD would show atypical WM microstructural development reflected by higher FA and lower RD in early childhood followed by lower rate of FA and RD changes later in childhood compared to children with TD in most of major tracts. DTI data from 31 children with ASD and 19 children with TD between 2 and 7 years of age was acquired. FA and RD were measured at core WM voxels to characterize the WM microstructural changes in ASD across all 48 major WM tracts. Different from existing whole brain WM characterization for children with ASD in this age group [Walker et al., 2012], the anatomical locations and

TABLE I. Age and clinical assessment scores of children with autism spectrum disorder (ASD)

	Median	Minimum	Maximum	Interquartile range
Age (year)	3.39	2.33	7.00	2.16
Clinical assessment score				
Autism Behavior Checklist	94.00	79.00	107.00	11.50
Autism Diagnostic Interview (ADI)	53.00	41.00	67.00	7.50
Childhood Autism Rating Scale (CARS)	41.00	36.00	50.00	3.50
Clancy Autism Behavior Scale (CABS)	18.00	14.00	22.00	2.00

distribution of atypically developmental WM voxels in all 48 WM tracts will be examined and presented in three-dimensionally (3D) reconstructed tracts. The FA or RD trend lines at these locations for both TD and ASD groups will be demonstrated. Furthermore, extent of atypical WM development within specific tract or tract group will be determined quantitatively.

MATERIALS AND METHODS

Children With ASD and Children With TD

All participants were male children recruited at Beijing Children's Hospital. About 31 children with ASD aged 2.33–7.00 years (4.11 ± 1.42 years) and 19 children with TD aged 1.99–6.83 years (4.00 ± 1.42 years) participated in this study. The 19 children with TD at the time of MR imaging were referred for seizures with fever (n = 8), intermittent headache (n = 9), and strabismus (n = 2). All these children with TD had normal neurological examinations documented in medical record. The exclusion criteria for children with TD include known nervous system disease, or history of psychiatric, neurodevelopmental or systemic illness. Children with ASD were not receiving any CNS-active medications before MRI studies. Namely, they were all medication naïve children with ASD at the scan. The diagnosis of ASD was established using the Autism Diagnostic Interview-Revised (ADI-R) [Lord et al., 1994], Childhood Autism Rating Scale (CARS), Clancy Autism Behavior Scale (CABS) [Clancy et al., 1969], and Autism Behavior Checklist [Krug et al., 1980], and diagnoses were confirmed based on expert opinion according to Diagnostic and Statistical Manual of Mental Disorder-Version IV-Text Revision (DSM-IV-TR) criteria [APA, 2000]. The detailed age and clinical assessment scores for children with ASD were provided in Table I. Every child's parents provided signed consent and the protocol was approved by Beijing Children's Hospital Research Ethics Committee.

Acquisition of DTI Image

All MR scans were performed on a 3T Philips Achieva Magnetic Resonance System with sedation. DTI data were acquired using a single-shot, echo-planar imaging (EPI) sequence with Sensitivity Encoding parallel imaging scheme (SENSE, reduction factor = 2). The imaging matrix size was 128×128 with a field of view (FOV) of 256×256 mm^2. Axial slices of 2 mm thickness were acquired parallel to the anterior–posterior commissure (AC–PC) line. A total of 70 slices covered the entire brain without a slice gap. The repetition time (TR) and echo time (TE) were 7.96 seconds and 83 milliseconds. Diffusion weighting was encoded along 30 independent directions and the b-value was 1000 s/mm^2. To increase the signal-to-noise ratio (SNR), two repetitions were performed.

DTI Tensor Fitting and Measurements of DTI-Derived Metrics

Automated image registration (AIR) [Woods et al., 1998] was applied to raw diffusion weighted images (DWI) to correct distortion caused by eddy current. Head motions in diffusion MRI data were quantified for all subjects (see characterization of motion in the DTI scans in Supporting Information Figure S1 and S2 for more details). Few motion artifacts were observed in the present DTI datasets. Supporting Information Figures S1 and S2 showed that volume translation was less than 0.5 mm and rotation was around 0.12° among DWI volumes. The standard tensor fitting was conducted with DTIStudio [Jiang et al., 2006] to generate the DTI-derived metrics, FA, and RD.

Parcellation of WM Into Tracts and Tract Groups

A deterministic digital WM atlas (JHU ICBM-DTI-81) [Mori et al., 2008] was used to parcellate WM into 48 major tracts with each tract having a discrete labeling from 1 to 48. These tracts were identified with unique numbers and further categorized into five tract groups including limbic, commissural, association, projection, and brainstem tract groups, for characterization of the WM microstructural changes at the level of tract group [Wakana et al., 2004].

Group Comparisons of FA and RD Between ASD and TD Groups With Voxel-Wise and Cluster Analysis

DTI measurements of ASD and TD groups were registered to ICBM-DTI-81 atlas space and compared at the

WM skeleton voxels to label the WM and effectively alleviate partial volume effects [Smith et al., 2006]. Nonlinear registration tool, FNIRT in FMRIB Software Library (FSL) (http://fsl.fmrib.ox.ac.uk/fsl/fslwiki/TBSS) package [Rueckert et al., 1999], was applied to register FA maps of all subjects to the EVE single-subject FA template [Huang et al., 2012a,b], for alignment to the JHU ICBM-DTI-81 atlas space. The registered FA maps of all subjects were averaged to generate a mean FA map, from which a FA skeleton mask was created. Skeletonized FA images of all subjects were obtained by projecting the registered FA images onto the mean FA skeleton mask. In the ICBM-DTI-81 atlas space, voxel-wise comparison was carried out with the skeletonized FA maps using permutation-based nonparametric statistics (Randomise, FSL tool; http://fsl.fmrib.ox.ac.uk/fsl/fslwiki/Randomise) with 5,000 permutations and the threshold free cluster enhancement (TFCE) [Smith and Nichols, 2009] method at cluster level threshold of $P<0.05$ corrected for multiple comparisons (TFCE-corrected). Age was entered into the voxel-wise statistics as a covariate to test group differences on FA or RD measurements. The WM labeling from the JHU ICBM-DTI-81 atlas was used to label each cluster to a corresponding WM tract. Similarly, RD values were projected onto the skeleton mask obtained from mean FA image and compared between ASD and TD groups with the procedures described above.

Comparisons of FA or RD maps between ASD and TD group were conducted for all participated children of 2–7 years (31 children with ASD and 19 children with TD) and a subgroup of children with less than 4 years of age (16 children with ASD and 13 children with TD).

Comparisons of Age-Dependent FA and RD Linear Trend Lines Between ASD and TD Groups

In addition to analysis of group differences, comparisons of age-dependent linear trend lines of the FA or RD measurements between ASD and TD groups were performed on all WM skeleton voxels in the ICBM-DTI-81 atlas space. Despite the cross-sectional nature in this study, age correlations provide a useful preliminary strategy for examining neurodevelopmental growth trajectories. General linear model (GLM), widely used for age-related trajectories, was applied to fit the age-dependent curves of the FA or RD and test differences of maturation rates of FA or RD between ASD and TD. Take FA measurement as an example. For FA measurement at any skeleton voxel from any participated subject, $FA_{i,j}$ was defined where i was the ith skeleton voxel, j denoted the participated child with ASD or TD. There were a total of M voxels in the skeleton and 50 subjects. Hence, i was from 1 to M and j was from 1 to 50. FA measurement for the skeleton voxel i of subject j can be constructed with mixed-effects model as follows:

$$FA_{i,j}=u_i+\beta_{1i}I_j+\beta_{2i}\tau_j+\beta_{3i}(I\alpha)_{ij}+\epsilon_{i,j} \quad (1)$$

where u_i was the overall mean of the FA measurements in ith voxel; I_j was the indicator variable with $I_j=1$ for ASD and $I_j=0$ for healthy control; τ_j represented the age of jth subject; $(I\alpha)_{ij}$ was the age-group interaction term and $\epsilon_{i,j}$ was the error term; β_{1i}, β_{2i}, and β_{3i} represent the parameters to be estimated for I_j, τ_j, and $(I\alpha)_{ij}$, respectively. In ith voxel, if the age-group interaction is significantly different from zero, the effect of age on FA measurements depends on group (ASD or TD), which means the age-dependence of FA in ith voxel are different between the ASD group and TD group. The statistical procedures were performed using R version 3.0.2 (http://www.r-project.org/).

We also confirmed no statistical difference between linear and nonlinear fitting of FA or RD trend lines (see Supporting Information Figure S3 and Table SI for comparisons of linear and nonlinear fitting). The findings in the Results section below are then based on linear fitting with GLM in R software. The clusters with atypical age-dependent FA or RD changes were first identified by voxels with significant age-group interaction (non-corrected $P<0.05$) in GLM. To correct for multiple comparisons, a small-volume correction with false discovery rate (FDR), which has been used in a previous autism study [Cheng et al., 2010], was conducted. Specifically, for each cluster selected in GLM described above, adjusted P-values were calculated for skeleton voxels in a small volume surrounding the cluster and consisting of skeleton voxels with 100 times the number of voxels of each cluster using FDR in R. Only clusters with continuous voxels >3 and $P<0.05$ (FDR corrected) were retained to avoid spurious results.

Quantifying the Extent of Atypical Age-Dependent Changes for Each WM Tract and Tract Group

To assess the extent of atypical age-dependent changes on each individual WM tract, an affected percentage index was calculated for each tract. As shown in Figure 1, by integrating the labeling of the individual WM tract in Figure 1B (e.g. genu of corpus callosum (GCC)) to the WM skeleton transformed into the atlas space (Fig. 1A), we can assign the skeleton WM voxels with major WM tract labels (Fig. 1C for GCC). In this way, the atlas labeling is overlaid to the mean skeleton in the JHU ICBM-DTI-81 space such that each skeleton voxel could be categorized into one of the major tracts. The tract (GCC in this example) from the atlas was 3D reconstructed in a transparent brain as anatomical guidance (Fig. 1D). The affected percentage of a tract was determined by the ratio between the skeleton voxel number of abnormal clusters in this tract and the total skeleton voxel number of this tract. Similarly, to assess the extent of the atypical age-dependent changes in each tract group, the affected

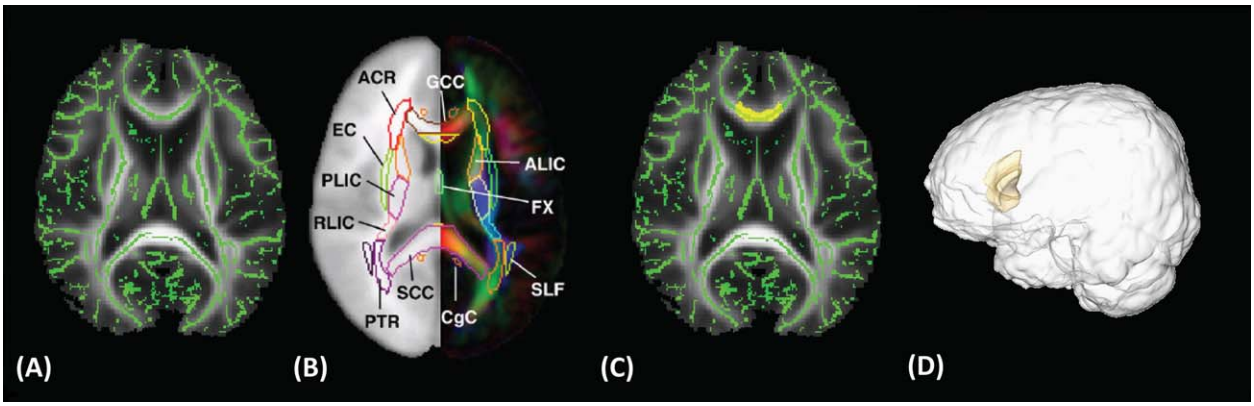

Figure 1.

Parcellation of core white matter (WM) into different tracts with a digital atlas. (A) Green skeleton representing core WM is overlaid on the averaged FA map; (B) the ICBM-DTI-81 digital WM atlas; (C) as an example, the genu of corpus callosum (GCC) (yellow) is transferred from the digital atlas to cover the green skeleton overlaid on the averaged FA map; (D) 3D depiction of GCC in reconstructed brain. See Supplemental Materials and Methods for abbreviation of the major WM tracts. *Abbreviations of commissural tracts*: BCC, body of corpus callosum; GCC, genu of corpus callosum; SCC, splenium of corpus callosum. *Abbreviations of limbic tracts*: BFX, body of fornix; CGC, cingulum bundle at cingulate gyrus; CGH, cingulum bundle at hippocampus; FX, fornix. *Abbreviations of projection tracts*: ACR, anterior corona radiata; ALIC, anterior limb of internal capsule; ATR, anterior thalamic radiation; CST, corticospinal tract; PCR, posterior corona radiata; PLIC, posterior limb of internal capsule; PTR, posterior thalamic radiation; RLIC, retrolenticular part of internal capsule; SCR, superior corona radiata. *Abbreviations of association tracts*: EC, external capsule; IFO, inferior fronto-occipital fasciculus; ILF, inferior longitudinal fasciculus; SFO, superior fronto-occipital fasciculus; SLF, superior longitudinal fasciculus; SLF (temporal part), superior longitudinal fasciculus (temporal part); SS, sagittal stratum; UNC, uncinate fasciculus. *Abbreviations of brainstem tracts*: CP, cerebellar peduncle; ICP, inferior cerebellar peduncle; MCP, middle cerebellar peduncle; ML, medial lemniscus; SCP, superior cerebellar peduncle. L and R indicate left and right, respectively.

percentage for a tract group was determined by the ratio between the skeleton voxel number of abnormal clusters in this tract group and the total skeleton voxel number of this tract group.

Age Intersection of ASD and TD Age-Dependent WM Trend Lines

As we hypothesized atypical WM microstructural developmental trend of WM tracts in ASD in the age of 2–7 years, we calculated the intersected age of two growth curves for each cluster voxel where atypical age-dependent change was found with FA or RD measurements of ASD and TD groups. Linear fitting was applied to all FA-age and RD-age fitting as there is no significant difference between linear and nonlinear (logarithmic) fitting (see Supporting Information Figure S3 and Table SI for comparisons of linear and nonlinear fitting). Take FA measurement as an example. After removing the age-group intersection term in Eq. (1), the separate linear fitting between FA measurements from ASD or TD groups and age was modeled as Eqs. (2.1) and (2.2), respectively.

$$FA_{i,ASDj} = u_{i,ASD} + \beta_{i,ASD}\tau_{ASDj} + \epsilon_{i,ASDj} \quad (2.1)$$

$$FA_{i,TDj} = u_{i,TD} + \beta_{i,TD}\tau_{TDj} + \epsilon_{i,TDj} \quad (2.2)$$

where i was the ith abnormal cluster, $ASDj$ or TDj denoted the participated child with ASD or TD; $u_{i,ASD}$ or $u_{i,TD}$ was the overall mean of the FA measurements in ith cluster in ASD group or TD group; τ_{ASDj} or τ_{TDj} represented the age of $ASDj$th or TDjth subject in each group; $\epsilon_{i,ASDj}$ and $\epsilon_{i,TDj}$ was the error term; and $\beta_{i,ASD}$ and $\beta_{i,TD}$ represented the parameters to be estimated for each cluster in each group. The intersected age $\tau_{i\_\text{intersect}}$ of the two fitted lines from ASD and TD group was calculated in Eq. (3) below:

$$\tau_{i\_\text{intersect}} = \frac{u_{i,ASD} - u_{i,TD}}{\beta_{i,TD} - \beta_{i,ASD}}. \quad (3)$$

Histograms of the intersected ages at the cluster voxels from FA and RD measurements were plotted.

RESULTS

Altered WM Microstructural Properties of Children With ASD Less Than 4 Years of Age

From Figure 2A and Table II, exclusively higher FA and exclusively lower RD were found for children with ASD

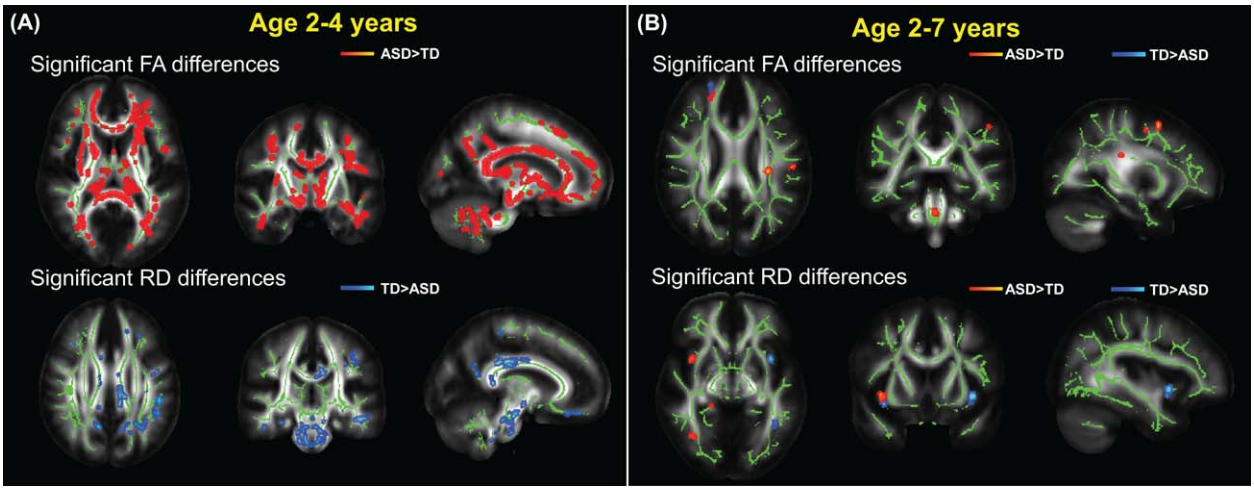

Figure 2.

Exclusively higher FA (red-yellow; upper panels) and lower RD (blue-cyan; lower panels) widely distributed in the WM were found in ASD less than 4 years of age, compared to age-matched TD (A); Bi-directional FA (red-yellow for one change direction and blue-cyan for another; upper panels) and RD (red-yellow for one change direction and blue-cyan for another; lower panels) changes sparsely distributed in the WM were found in ASD of 2–7 years of age compared to age-matched TD. Voxels with statistically significant FA or RD differences between ASD and TD are displayed in red-yellow (ASD>TD) or in blue-cyan (TD > ASD). WM skeleton voxels are shown in green. In (A) or (B), axial, coronal, and sagittal views are shown from left to right.

of 2–4 years of age compared to age-matched children with TD, suggesting altered WM microstructural properties for children with ASD before 4 years of age. On the contrary, differences of FA and RD between ASD and TD groups have two directions when the age range expands from 2–4 years to 2–7 years, as shown in Figure 2B and Table III. The mixed WM microstructural changes indicate age-dependent ASD effects, which can be further delineated with the atypical age-dependent WM microstructural trend lines described below.

Atypical Age-Dependent Microstructural Linear Trend Lines Widely Distributed in WM of ASD

Atypical age-dependent WM microstructural linear trend lines of ASD compared to those of TD were observed in widespread clusters distributed in multiple tracts of all five tract groups, limbic (Fig. 3A), association (Fig. 3B), brainstem (Fig. 4A), commissural (Fig. 4B), and projection (Fig. 4C) tract group. The progressive increase of FA values averaged from the largest cluster in each affected tract were observed for TD group with significant correlations ($P<0.05$ for all scatter plots in the left panels in Figs. 3 and 4) between FA and age, while flattened developmental trend lines (reduced WM microstructural maturation with age) of FA values were observed for ASD group with no significant correlation ($P>0.05$) for most scatter plots in the left panels in Figures 3 and 4 between FA and age. Similarly, progressive RD decreases in TD group and flattened RD trend lines in ASD group were found for another set of clusters also widely distributed in WM of all five tract groups, shown in scatter plots in the right panels of Figures 3 and 4. The atypical WM FA or RD age-dependent trend lines of ASD are nonparallel or overlapping to those of TD, resulting in the crossing of the trend lines, shown in the scatter plots of Figures 3 and 4. In addition, these FA or RD change rate differences are significant for all displayed clusters in the 3D images of Figures 3 and 4 with FDR-corrected P values less than 0.05. For example, FDR-corrected P value is 0.011 for FA change rate difference between ASD and TD in the cluster at GCC (left panel in Fig. 4B). FDR-corrected P value is less than 0.001 for RD change rate difference between ASD and TD in the cluster at left cerebellar peduncle (CP-L) (right panel in Fig. 4A). The percentages of voxels with atypical age-dependent microstructural changes inside each WM tract are shown in the bar plots of Figures 3 and 4.

Heterogeneous Extent of WM Clusters With Atypical Age-Dependent Microstructural Trend Lines Within Each Tract Group and Among Different Tract Groups

While it is consistent that slower change rates of FA and RD of ASD were observed for the clusters in all affected WM tracts, the extents and distributions of these clusters were evidently varied across different tracts of each tract group, as shown in bar plots in Figures 3 and 4. Moreover, the extents of the clusters with atypical age-dependent microstructural trend lines in ASD group were varied

TABLE II. FA (A) and RD (B) values (mean ± standard deviation), number of voxels, t, and *P* values of the identified largest cluster in each affected WM tract from group comparison of FA (A) and RD (B) at skeleton voxels between ASD and TD subgroups with age less than 4 years. L and R indicate left and right, respectively. See legend of Figure 1 for WM tract abbreviations

White matter tract	FA of TD (n=13)	FA of ASD (n=16)	# of Voxels	t	*P*
ASD>TD from FA measurements					
Commissural tract group					
Forceps major	0.51 ± 0.03	0.54 ± 0.03	1738	2.77	0.0100
Forceps minor	0.47 ± 0.03	0.49 ± 0.03	2973	2.14	0.0413
Limbic s stem tract group					
CGC-R	0.46 ± 0.04	0.52 ± 0.06	14	3.19	0.0036
CGC-L	0.44 ± 0.04	0.47 ± 0.03	359	2.78	0.0098
CGH-R	0.41 ± 0.03	0.45 ± 0.06	55	2.47	0.0199
CGH-L	0.41 ± 0.02	0.43 ± 0.04	203	2.70	0.0119
Projection tract group					
ATR-R	0.40 ± 0.01	0.42 ± 0.02	1459	2.23	0.0345
ATR-L	0.37 ± 0.02	0.38 ± 0.02	2155	2.14	0.0415
CST-R	0.56 ± 0.02	0.57 ± 0.02	1153	2.67	0.0126
CST-L	0.57 ± 0.02	0.58 ± 0.02	705	2.40	0.0235
Association tract group					
IFO-R	0.42 ± 0.03	0.44 ± 0.03	2111	2.26	0.0323
IFO-L	0.41 ± 0.02	0.43 ± 0.02	2403	2.66	0.0129
ILF-R	0.42 ± 0.02	0.44 ± 0.02	1026	2.06	0.0493
ILF-L	0.39 ± 0.02	0.42 ± 0.02	1465	2.97	0.0062
SLF-R	0.42 ± 0.02	0.44 ± 0.02	1216	2.75	0.0104
SLF-L	0.40 ± 0.02	0.43 ± 0.02	2475	3.83	0.0007
UNC-R	0.42 ± 0.03	0.44 ± 0.03	358	2.60	0.0150
UNC-L	0.39 ± 0.03	0.42 ± 0.02	903	2.67	0.0128
SLF (temporal part)-R	0.45 ± 0.02	0.47 ± 0.02	530	2.39	0.0242
SLF (temporal part)-L	0.43 ± 0.02	0.45 ± 0.02	1379	3.35	0.0024
Brainstem tract group					
MCP	0.57 ± 0.03	0.60 ± 0.03	256	2.23	0.0342
ML-R	0.40 ± 0.04	0.44 ± 0.04	48	2.19	0.0372
ML-L	0.43 ± 0.04	0.46 ± 0.03	51	2.23	0.0355
SCP-R	0.67 ± 0.03	0.69 ± 0.03	56	2.37	0.0258
CP-R	0.53 ± 0.05	0.57 ± 0.05	14	2.17	0.0392
CP-L	0.63 ± 0.04	0.66 ± 0.03	95	2.75	0.0109

White matter tract	RD ($\times 10^{-3}$ mm^2/s) of TD (n=13)	RD ($\times 10^{-3}$ mm^2/s) of ASD (n=16)	# of Voxels	t	*P*
ASD<TD from RD measurements					
Commissural tract group					
Forceps major	0.59 ± 0.04	0.56 ± 0.04	1670	2.30	0.0293
Limbic s stem tract group					
CGC-R	0.62 ± 0.05	0.57 ± 0.04	13	3.22	0.0033
CGC-L	0.61 ± 0.04	0.59 ± 0.04	304	2.07	0.0486
CGH-R	0.65 ± 0.05	0.61 ± 0.06	36	2.18	0.0379
CGH-L	0.64 ± 0.03	0.62 ± 0.04	175	2.22	0.0352
Projection tract group					
ATR-R	0.64 ± 0.03	0.61 ± 0.02	1373	2.86	0.0080
ATR-L	0.65 ± 0.03	0.62 ± 0.02	1823	2.54	0.0172
CST-R	0.51 ± 0.03	0.49 ± 0.03	1161	2.19	0.0375
CST-L	0.50 ± 0.03	0.48 ± 0.03	972	2.08	0.0473
Association tract group					
IFO-R	0.63 ± 0.04	0.61 ± 0.03	614	2.32	0.0283

TABLE II. (continued).

White matter tract	RD ($\times 10^{-3}$ mm^2/s) of TD (n=13)	RD ($\times 10^{-3}$ mm^2/s) of ASD (n=16)	# of Voxels	t	*P*
IFO-L	0.65 ± 0.04	0.63 ± 0.03	2249	2.12	0.0435
ILF-L	0.66 ± 0.04	0.63 ± 0.03	1446	2.23	0.0345
SLF-L	0.63 ± 0.03	0.61 ± 0.03	2319	2.29	0.0300
UNC-R	0.60 ± 0.04	0.58 ± 0.04	173	2.31	0.0291
UNC-L	0.68 ± 0.05	0.65 ± 0.04	64	2.37	0.0249
SLF (temporal part)-L	0.62 ± 0.03	0.60 ± 0.03	1260	2.13	0.0428
Brainstem tract group					
MCP	0.50 ± 0.04	0.45 ± 0.04	171	3.21	0.0036
ML-R	0.51 ± 0.03	0.49 ± 0.03	74	2.26	0.0335
SCP-R	0.41 ± 0.03	0.39 ± 0.02	75	2.83	0.0093
CP-R	0.48 ± 0.03	0.44 ± 0.03	127	3.59	0.0013
CP-L	0.48 ± 0.04	0.43 ± 0.03	116	3.63	0.0014

among different tract groups, as shown in Figure 5A,C. Specifically, based on both FA and RD measurements, the limbic and association tract groups were more severely affected with higher percentage of WM voxels with atypical age-dependent microstructural trend lines while brainstem, commissural, and projection tract groups were less severely affected. The exact percentage values of WM voxels with atypical age-dependent trend lines in ASD within each tract or each tract group from FA or RD measurements are listed in Table SII of supplemental information.

Distributions of the Intersected Ages of Age-Dependent WM Linear Trend Lines of Children With ASD and TD

With intersections of FA or RD curves of ASD and those of TD clearly observed in all tract groups (Figs. 3 and 4), the distribution of the ages of these intersections is demonstrated in Figure 5B,D. Most trend lines intersections occurred around 4 years with both FA (3.93 ±0.39 years) and RD measurements (4.00 ± 0.66 years).

DISCUSSION

Atypical age-dependent WM microstructural changes of children with ASD revealed by surveying all WM tracts and tract groups offer comprehensive information for understanding WM developmental pattern affected by ASD. Specifically, the results suggest that early atypical microstructural development was reflected by higher FA and lower RD in most major WM tracts in ASD group before 4 years of age followed by reduced rates of tract maturation through 7 years of age (Figs. 2–4). Furthermore, the atypical age-dependent WM microstructural changes are heterogeneous among different WM tract groups with more prominent atypical developmental patterns observed in limbic and association tracts, compared to brainstem, commissural, and projection tracts (Fig. 5A,C). The present study attempts to systematically determine the anatomical location, distribution, and extent of atypical age-dependent trend lines across all major WM tracts and tract groups in young children with ASD. With each individual WM tract forming the neuroanatomical basis of global and local brain circuits, these findings provide important new evidence to understand the pattern and timing of atypical WM development in ASD with implications for how they might contribute to alterations in the circuit level organization of brain function and behavior. The comprehensive results from group comparisons at different age ranges and trajectory analyses may also help elucidate the seemingly nonuniform WM finding of children with ASD, as different patterns of WM microstructural abnormality appear to be present at different ages [e.g. Ben Bashat et al., 2007; Kumar et al., 2010; Sundaram et al., 2008; Walker et al., 2012; Weinstein et al., 2011; Wolff et al., 2012]. Integration of WM skeleton and tract parcellation (Fig. 1) that effectively alleviated the partial volume effects and revealed the anatomical locations in the context of WM tracts offered technical advantage of this study.

With FA inferring the overall WM microstructural integrity [Beaulieu, 2002] and RD being more specific to quantitatively inferring WM myelination [Song et al., 2005], group comparisons of WM FA or RD with age as a covariate yielded results showing WM microstructural changes in both directions (Fig. 2B); on the other hand, the exclusively higher FA and lower RD was found for children with ASD less than 4 years of age (Fig. 2A). In light of identified trend line intersection ages shown in Figure 5B,D, the bi-directional results in Figure 2B could come from mixed effects of early higher FA and lower RD by 4 years (Fig. 2A) and slower FA and RD changes from 2 to 7 years of age. The results of Figure 2A,B combined with the revealed age-dependent microstructural trend lines in Figures 3 and 4 may shed light on the nonuniform WM findings for children with ASD at this age range (2–7 years) in the literature [e.g. Ben Bashat et al., 2007; Kumar et al., 2010; Sundaram et al., 2008; Walker et al., 2012; Weinstein

TABLE III. FA (A) and RD (B) values (mean ± standard deviation), number of voxels, t, and *P* values of the identified largest cluster in each affected WM tract from group comparison of FA (A) and RD (B) at skeleton voxels between ASD and TD group of all subjects with age of 2 to 7 years. L and R indicate left and right, respectively. See legend of Figure 1 for WM tract abbreviations

White matter tract	FA of TD (n=19)	FA of ASD (n=31)	# of voxels	t	*P*
ASD>TD from FA measurements					
Commissural tract group					
Forceps minor	0.27 ± 0.02	0.30 ± 0.03	121	2.93	0.0055
Forceps minor	0.26 ± 0.04	0.29 ± 0.04	29	2.18	0.0345
Limbic s stem tract group					
CGC-R	0.28 ± 0.05	0.33 ± 0.05	32	2.89	0.0060
CGC-R	0.23 ± 0.04	0.27 ± 0.05	14	2.86	0.0064
Projection tract group					
ATR-L	0.32 ± 0.03	0.36 ± 0.03	155	3.85	0.0004
CST-R	0.51 ± 0.03	0.53 ± 0.04	18	2.10	0.0415
CST-R	0.41 ± 0.03	0.44 ± 0.06	15	2.33	0.0235
ATR-R	0.29 ± 0.02	0.31 ± 0.02	12	2.70	0.0096
Association tract group					
UNC-L	0.30 ± 0.02	0.32 ± 0.02	69	2.15	0.0372
SLF-L	0.34 ± 0.03	0.38 ± 0.04	55	3.53	0.0009
SLF-L	0.26 ± 0.04	0.31 ± 0.05	16	2.60	0.0126
IFO-R	0.26 ± 0.07	0.31 ± 0.07	11	2.31	0.0257
ASD<TD from FA measurements					
Association tract group					
SLF-R	0.37 ± 0.09	0.31 ± 0.09	13	2.48	0.0174

White matter tract	RD ($\times 10^{-3}$mm^2/s) of TD (n=19)	RD ($\times 10^{-3}$mm^2/s) of ASD (n=31)	# of voxels	t	*P*
ASD<TD from RD measurements					
Limbic s stem tract group					
CGC-R	0.68 ± 0.04	0.64 ± 0.04	59	2.86	0.0068
Projection tract group					
CST-R	0.73 ± 0.10	0.66 ± 0.05	10	2.53	0.0181
Association tract group					
UNC-R	0.88 ± 0.10	0.82 ± 0.10	18	2.03	0.0490
IFO-R	0.71 ± 0.06	0.67 ± 0.07	11	2.36	0.0224
ASD>TD from RD measurements					
Limbic s stem tract group					
CGH-L	0.61 ± 0.07	0.67 ± 0.10	11	2.38	0.0213
Association tract group					
SLF-R	0.64 ± 0.07	0.69 ± 0.07	12	2.21	0.0325
IFO-R	0.75 ± 0.03	0.79 ± 0.03	11	3.72	0.0006

et al., 2011; Wolff et al., 2012]. That is, higher FA and lower RD before a certain age and reduced rate of changes of these two metrics after that age in individuals with ASD may result in the seemingly nonuniform results. It suggests an age window, even a narrow one, may play a critical role for elucidating nuanced developmental differences associated with ASD.

DTI offers microstructural measurements of FA and RD to access WM maturational process. Progressive FA increases and RD decreases have been found in normal WM maturational process in childhood [Lebel and Beaulieu, 2011]. Figures 3 and 4 inferred high level of WM microstructural maturation for children with ASD until around 4–5 years of age but the maturation progressed more slowly after that age. Namely, FA or RD of widespread WM in all five major tract groups for children with ASD before 4–5 years of age reached to a level equivalent to that of older children with TD (Figs. 3 and 4). By combining the group comparison analysis and analysis of interaction of age-dependent microstructural trend lines, we were able to document the widespread nature of early WM microstructural alterations in ASD compared to TD, the intersection point at which WM growth in TD individuals catches up to that growth, and the early phase of

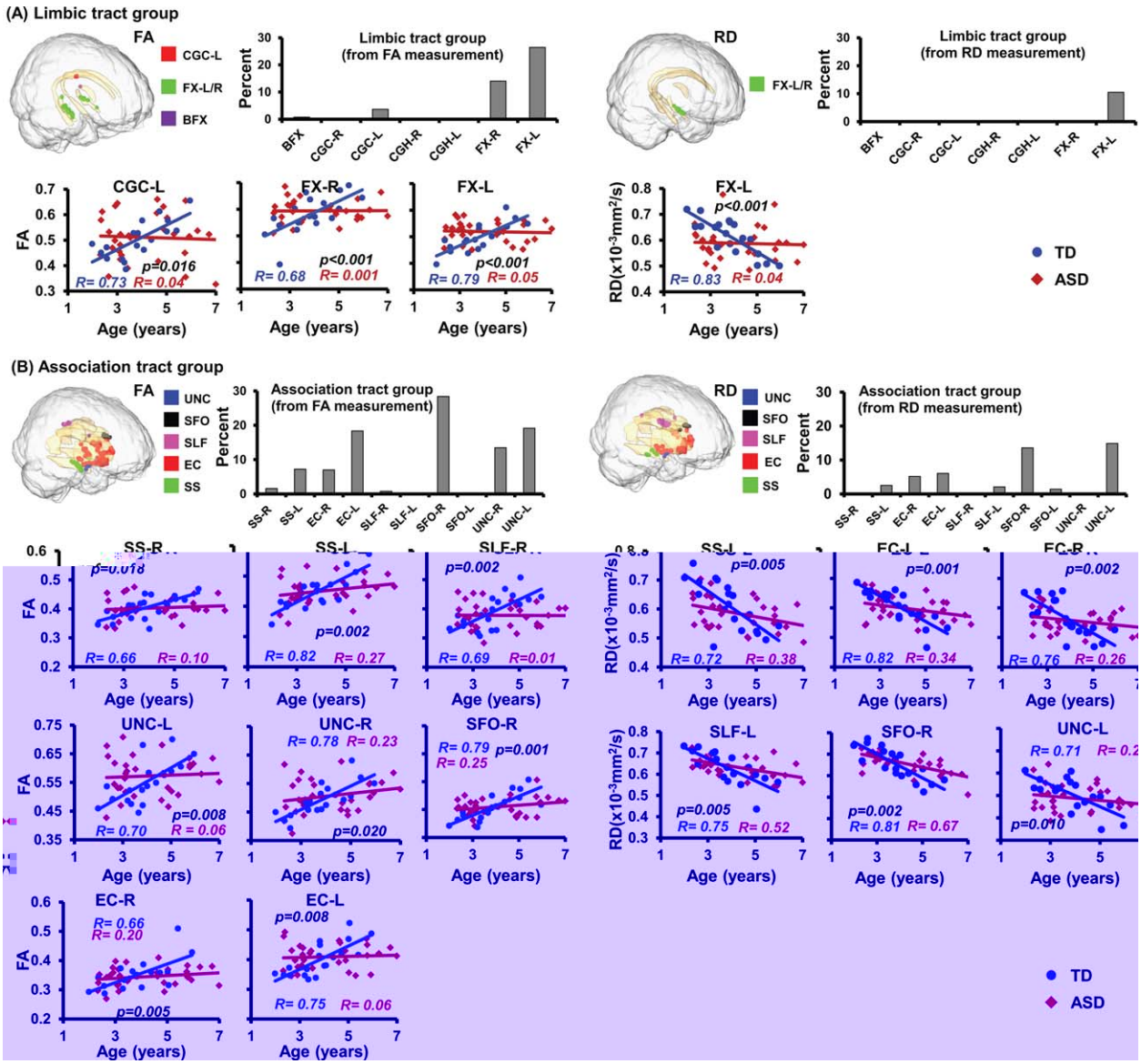

Figure 3.

Clusters with significant age-group interactions in the limbic system (A) and association tract group (B) with FA and RD measurements. The locations and distributions of significant clusters in reconstructed limbic tracts (A) and association tracts (B) (light yellow and directly from the digital WM atlas) are visualized in 3D in the top left panel of each measurement. Significant clusters in different limbic tracts (A) and association tract (B) are coded with different colors, also shown in the top left panel of each measurement. The entire brain (gray) is also shown as anatomical reference. The percentage values of affected voxels within each limbic tract (A) and association tract (B) are shown in the bar plots in the top right panel of each measurement. Scatter plots of FA or RD averaged from the largest cluster of atypical age-dependent WM changes in each affected limbic tract (A) and association tract (B) are shown in lower panels for children with ASD and TD. Each red diamond or blue circle in the scatter plot represents FA or RD measurement from one child with ASD or TD, respectively. The solid lines (blue for TD and red for ASD) were linearly fitted from these measurements. R values (blue for TD and red for ASD) are correlation coefficients of FA or RD measurements and age. FDR-corrected *P* value in each scatter plot indicates the difference of trend line rate of these metrics between ASD and TD groups. L and R indicate left and right, respectively. See legend of Figure 1 for WM tract abbreviations.

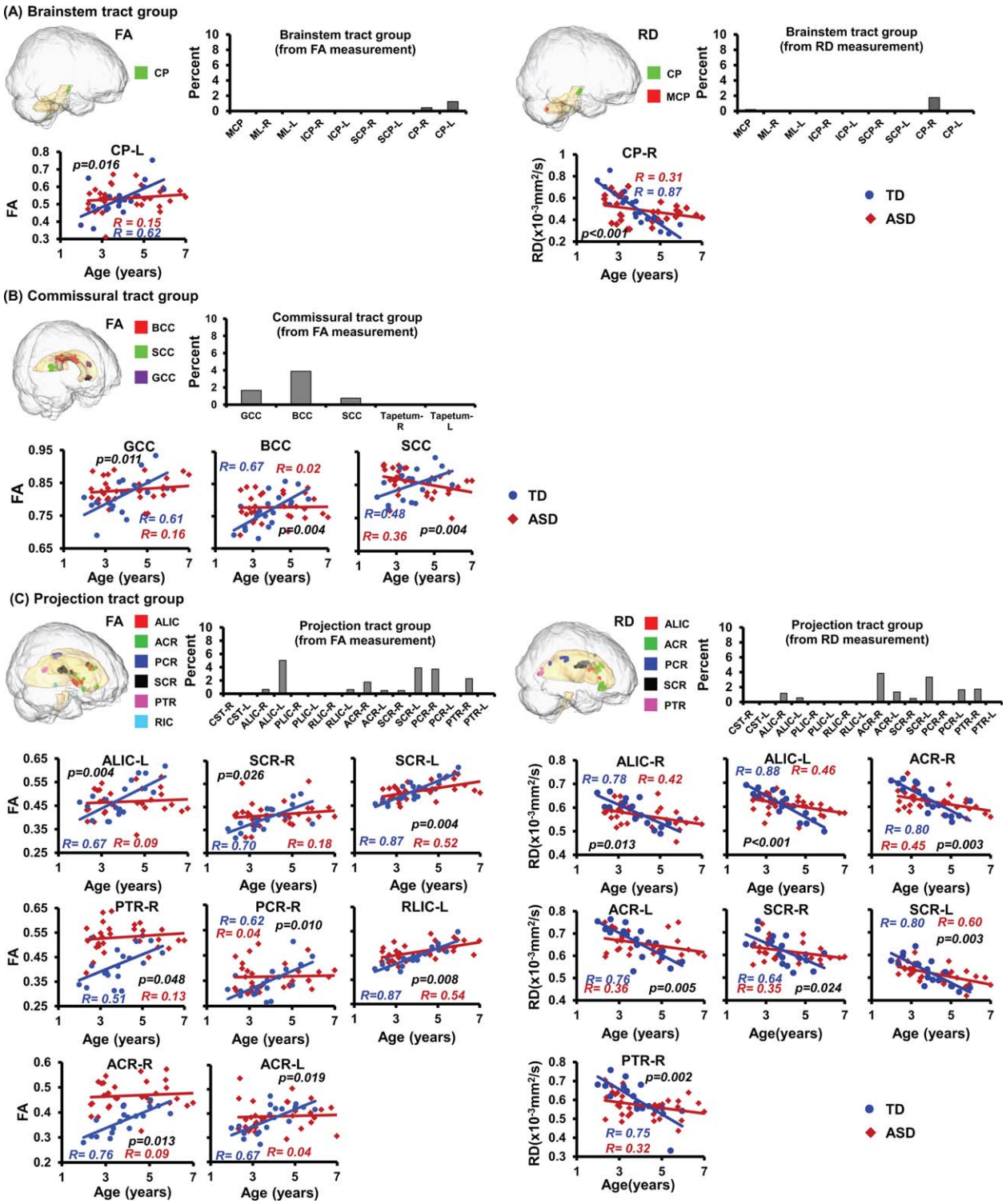

Figure 4.

Clusters with significantly age-group interactions in the brainstem (A), commissural (B), and projection tract group (C) with FA and RD measurements. See legend of Figure 3 for details.

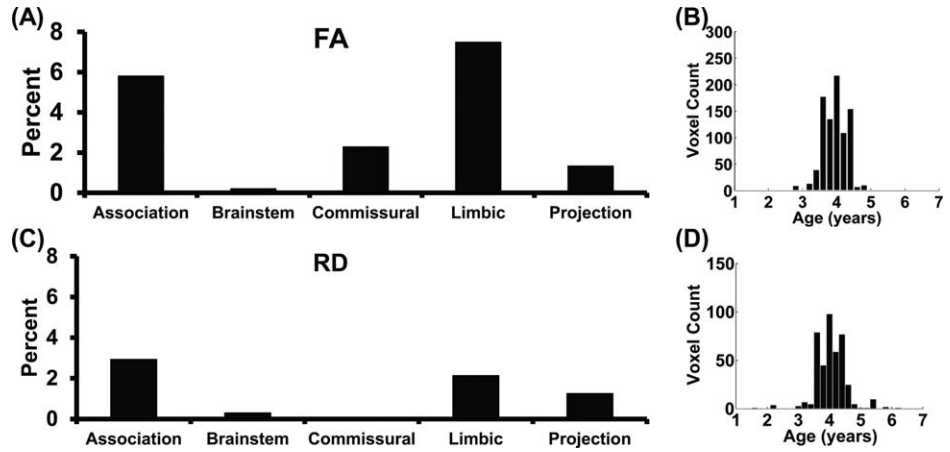

Figure 5.

The percentage values of affected voxels within each WM tract group for FA (A) and RD (C) measurements of five major tract groups. (B) and (D) demonstrate the histograms of ages from intersections of linear trend lines of FA (B) and RD (D) measurements of children with ASD and those with TD, respectively.

brain growth beyond 4 years of age that leads to the pattern of lower FA and higher RD in ASD from late childhood to adulthood.

The widespread locations of atypical age-dependent linear trend lines in all five WM tract groups of children with ASD are possibly related to the feature of ASD as a heterogeneous spectrum disorder with a wide range of symptom severity. It affects brain functions in multiple aspects including social impairment, communication deficits, and repetitive behaviors [Lord et al., 1994; Amaral et al., 2008]. The atypical age-dependent trend lines are especially prominent in the limbic and association tract groups (Fig. 5A,C). Alterations in trend lines of limbic WM tract (Fig. 3A) may explain disruption of limbic circuitry [e.g. Haznedar et al., 2000] and some clinical manifestations of ASD [e.g. Bauman and Kemper, 1987] that lead to reduced social learning experiences and impaired social development [e.g. Dawson et al., 2004]. Left superior longitudinal fasciculus (SLF), as a major association tract, connects between Broca's area and Wernicke's area, both related to language. The alterations of microstructural trajectory of FA and RD in left SLF in Figure 3B suggest abnormality in myelin development and might be related to slower neural transmission [Shukla et al., 2011] and therefore the impairment of language development seen in some children with ASD [e.g. Weinstein et al., 2011]. Atypical age-dependent microstructural trend lines of the superior fronto-occipital fasciculus (SFO) and the uncinate fasciculus (UNC) (Fig. 3B) may contribute to impairment of attention, emotion processing, memory, and language functions which these two tracts are involved with [Catani and Thiebaut de Schotten, 2008; Radua et al., 2011]. Less prominent atypical age-dependent trend lines of children with ASD were found in brain stem, commissural, and projection tracts (Fig. 5A,C), however, clusters of significant trend line differences between children with ASD and those with TD were found in these tract groups too (Fig. 4). Previous autism study reported cerebellar dysfunction affected the establishment of neural circuitry [e.g. Allen, 2005; Mosconi et al., 2015] involving cerebellar peduncle (CP) and we also found atypical age-dependent WM changes in CP (Fig. 4A). The atypical microstructural development in corpus callosum (CC) (shown in Fig. 4B), as the large commissural tract, has been probably mostly reported in previous autism studies [e.g. Alexander et al., 2007; Barnea-Goraly et al., 2005]. The involved projection tracts (Fig. 4C) including internal capsule (IC) and corona radiata (CR) are related to perceptual, motor functions and other higher cognitive functions [Schmahmann and Pandya, 2008] known to be impaired in ASD [e.g. Mosconi et al., 2015].

Several limitations and considerations of the present study are elaborated here. First, while the present WM microstructural findings further develop and are consistent with the view that there is an atypical pattern of brain development in ASD, the age-dependent FA or RD curves came from cross-sectional datasets, but not longitudinal datasets from either children with ASD or children with TD. Relevantly the distribution of ages from the crossings of the fitted linear trend lines in Figure 5B,D cannot be interpreted as the crossings of real trajectories, either. Hence, the intersections of the fitted trend lines are indirect indication of crossed ages and also depend on the model selected (see Supporting Information Figure S3 and Table SI for selection of curve fitting model). Stronger confirmation of the FA or RD trajectories and crossed ages between children with ASD and those of TD will come from future longitudinal studies [see e.g. Hedman et al.,

2012 for review of longitudinal brain volume measurements and Lebel and Beaulieu, 2011 for longitudinal trajectories of FA and MD). In addition, for characterizing a heterogeneous neurodevelopmental disorder, the sample size is relatively small for entire ASD and TD group, especially for TD subgroup over 4 years of age. The challenge is related to the difficulty of recruitment of subjects in this age range, especially children with TD. Therefore, group comparisons were conducted with FA or RD measurements for children of entire group with age range of 2–7 years and subgroup of children with age less than 4 years, but not for subgroup of children with age over 4 years. Future studies of direct comparison in the cohorts over 4 years with larger sample size may further support the importance of age of 4 years as a possible turning point reversing the direction of group comparison outcomes across different age ranges. Specially, lower FA and higher RD for children with ASD in age of 4–7 years would be expected, given a larger sample size. FA and RD also reflect other factors such as axon packing [Madler et al., 2008] or axon density [Klawiter et al., 2011]. An alternative explanation of higher FA for children with ASD at the age of less than 4 years might then be higher axon density instead of enhanced myelination. However, caution needs to be taken to interpret results of FA and RD which are used to infer the WM microstructure, but are not direct measures of axonal density, axonal packing or myelin level [Wheeler-Kingshott and Cercignani, 2009].

In conclusion, we identified microstructural alterations in widely distributed multiple WM tracts, particularly in associational and limbic tracts, in children with ASD before 4 years of age and a reduced rate of WM maturation after that age. With WM tracts underlying brain circuits and connectivity, characterizing the atypical age-dependent WM trend lines, specifically the anatomical locations, distribution, and extent of the affected WM within specific tracts and tract groups, have potential implications for identifying children at highest risk for ASD and targeted preventive interventions.

ACKNOWLEDGMENTS

The authors are grateful to Austin Ouyang for discussion on data analysis and 3D visualization. The authors report no biomedical financial interests or potential conflicts of interest.

REFERENCES

Alexander AL, Lee JE, Lazar M, Boudos R, DuBray MB, Oakes TR, Miller JN, Lu J, Jeong EK, McMahon WM, Bigler ED, Lainhart JE (2007): Diffusion tensor imaging of the corpus callosum in autism. Neuroimage 34:61–73.

Allen G (2005): The cerebellum in autism. Clin Neuropsychiatry 2: 321–337.

Amaral DG, Schumann CM, Nordahl CW (2008): Neuroanatomy of autism. Trends Neurosci 31:137–145.

APA (2000): Diagnostic and Statistical Manual of Mental Disorders, 4th ed. Washington, DC: American Psychiatric Association.

Baird G, Cass H, Slonims V (2003): Diagnosis of autism. BMJ 327: 488–493.

Barnea-Goraly N, Menon V, Eckert M, Tamm L, Bammer R, Karchemskiy A, Dant CC, Reiss AL (2005): White matter development during childhood and adolescence: A cross-sectional diffusion tensor imaging study. Cereb Cortex 15:1848–1854.

Basser PJ, Mattiello J, LeBihan D (1994): MR diffusion tensor spectroscopy and imaging. Biophys J 66:259–267.

Bauman, M, Kemper, T (1987): Limbic involvement in a second case of early infantile autism. Neurology 37:147

Beaulieu C (2002): The basis of anisotropic water diffusion in the nervous system–A technical review. NMR Biomed 15:435–455.

Ben Bashat D, Kronfeld-Duenias V, Zachor DA, Ekstein PM, Hendler T, Tarrasch R, Even A, Levy Y, Ben Sira L (2007): Accelerated maturation of white matter in young children with autism: A high b value DWI study. Neuroimage 37:40–47.

Casey B, Tottenham N, Liston C, Durston S (2005): Imaging the developing brain: What have we learned about cognitive development? Trends Cogn Sci 9:104–110.

Catani M, Thiebaut de Schotten M (2008): A diffusion tensor imaging tractography atlas for virtual in vivo dissections. Cortex 44:1105–1132.

Cheng Y, Chou KH, Chen IY, Fan YT, Decety J, Lin CP (2010): Atypical development of white matter microstructure in adolescents with autism spectrum disorders. Neuroimage 50:873–882.

Clancy H, Dugdale A, Rendle-Short J (1969): The diagnosis of infantile autism. Dev Med Child Neurol 11:432–442.

Courchesne E, Pierce K, Schumann CM, Redcay E, Buckwalter JA, Kennedy DP, Morgan J (2007): Mapping early brain development in autism. Neuron 56:399–413.

Daniels AM, Mandell DS (2013): Explaining differences in age at autism spectrum disorder diagnosis: A critical review. Autism 18:583–597.

Dawson G, Toth K, Abbott R, Osterling J, Munson J, Estes A, Liaw J (2004): Early social attention impairments in autism: Social orienting, joint attention, and attention to distress. Dev Psychol 40:271–283.

Haznedar MM, Buchsbaum MS, Wei TC, Hof PR, Cartwright C, Bienstock CA, Hollander E (2000): Limbic circuitry in patients with autism spectrum disorders studied with positron emission tomography and magnetic resonance imaging. Am J Psychiatry 157:1994–2001.

Hedman AM, van Haren NE, Schnack HG, Kahn RS, Pol H, Hilleke E (2012): Human brain changes across the life span: A review of 56 longitudinal magnetic resonance imaging studies. Hum Brain Mapp 33:1987–2002.

Huang H, Fan X, Weiner M, Martin-Cook K, Xiao G, Davis J, Devous M, Rosenberg R, Diaz-Arrastia R (2012a): Distinctive disruption patterns of white matter tracts in Alzheimer's disease with full diffusion tensor characterization. Neurobiol Aging 33:2029–2045.

Huang H, Gundapuneedi T, Rao U (2012b): White matter disruptions in adolescents exposed to childhood maltreatment and vulnerability to psychopathology. Neuropsychopharmacology 37:2693–2701.

Jiang H, van Zijl PC, Kim J, Pearlson GD, Mori S (2006): DtiStudio: Resource program for diffusion tensor computation and fiber bundle tracking. Comput Methods Programs Biomed 81: 106–116.

Kanner L (1968): Autistic disturbances of affective contact. Acta Paedopsychiatr 35:100–136.

Klawiter EC, Schmidt RE, Trinkaus K, Liang H, Budde MD, Naismith RT, Song S, Cross AH, Benzinger TL (2011): Radial diffusivity predicts demylination in ex vivo multiple sclerosis spinal cords. Neuroimage 55:1454–1460.

Krug DA, Arick J, Almond P (1980): Behavior checklist for identifying severely handicapped individuals with high levels of autistic behavior. J Child Psychol Psychiatry 21:221–229.

Kumar A, Sundaram SK, Sivaswamy L, Behen ME, Makki MI, Ager J, Janisse J, Chugani HT, Chugani DC (2010): Alterations in frontal lobe tracts and corpus callosum in young children with autism spectrum disorder. Cereb Cortex 20:2103–2113.

Lebel C, Beaulieu C (2011): Longitudinal development of human brain wiring continues from childhood into adulthood. J Neurosci 31:10937–10947.

Lord C, Rutter M, Le Couteur A (1994): Autism diagnostic interview-revised: A revised version of a diagnostic interview for caregivers of individuals with possible pervasive developmental disorders. J Autism Dev Disord 24:659–685.

Malder B, Drabycz SA, Kolind SH, Whittall KR, MacKay AL (2008): Is diffusion anisotropy an accurate monitor of myelination? Correlation of multicompoent T_2 relaxation and diffusion tensor anisotropy in human brain. Mag Res Imag 26:874–888.

Mori S, Crain BJ, Chacko VP, van Zijl PC (1999): Three-dimensional tracking of axonal projections in the brain by magnetic resonance imaging. Ann Neurol 45:265–269.

Mori S, Oishi K, Jiang H, Jiang L, Li X, Akhter K, Hua K, Faria AV, Mahmood A, Woods R, Toga AW, Pike GB, Neto PR, Evans A, Zhang J, Huang H, Miller MI, van Zijl P, Mazziotta J (2008): Stereotaxic white matter atlas based on diffusion tensor imaging in an ICBM template. Neuroimage 40:570–582.

Mosconi MW, Mohanty S, Greene RK, Cook EH, Vaillancourt DE, Sweeney JA (2015): Feedforward and feedback motor control abnormalities implicate cerebellar dysfunctions in autism spectrum disorder. J Neurosci 35:2015–2025.

Paus T, Keshavan M, Giedd JN (2008): Why do many psychiatric disorders emerge during adolescence? Nature Rev Neurosci 9: 947–957.

Penagarikano O, Abrahams BS, Herman EI, Winden KD, Gdalyahu A, Dong H, Sonnenblick LI, Gruver R, Almajano J, Bragin A, Golshani P, Trachtenberg JT, Peles E, Geschwind DH (2011): Absence of CNTNAP2 leads to epilepsy, neuronal migration abnormalities, and core autism-related deficits. Cell 147:235–246.

Radua J, Via E, Catani M, Mataix-Cols D (2011): Voxel-based meta-analysis of regional white-matter volume differences in autism spectrum disorder versus healthy controls. Psychol Med 41:1539–1550.

Rueckert D, Sonoda LI, Hayes C, Hill DLG, Leach MO, Hawkes DJ (1999): Nonrigid registration using free-form deformations: Application to breast MR images. IEEE Trans Med Imaging 18: 712–721.

Schmahmann JD, Pandya DN (2008): Disconnection syndromes of basal ganglia, thalamus, and cerebrocerebellar systems. Cortex 44:1037–1066.

Shukla DK, Keehn B, Smylie DM, Muller RA (2011): Microstructural abnormalities of short-distance white matter tracts in autism spectrum disorder. Neuropsychologia 49:1378–1382.

Smith SM, Jenkinson M, Johansen-Berg H, Rueckert D, Nichols TE, Mackay CE, Watkins KE, Ciccarelli O, Cader MZ, Matthews PM, Behrens TE (2006): Tract-based spatial statistics: voxelwise analysis of multi-subject diffusion data. Neuroimage 31:1487–1505.

Smith SM, Nichols TE (2009): Threshold-free cluster enhancement: Addressing problems of smoothing, threshold dependence, and localisation in cluster inference. Neuroimage 44:83–98.

Song SK, Yoshino J, Le TQ, Lin SJ, Sun SW, Cross AH, Armstrong RC (2005): Demyelination increases radial diffusivity in corpus callosum of mouse brain. Neuroimage 26:132–140.

Sowell ER, Bookheimer SY (2012): Promise for finding brain biomarkers among infants at high familial risk for developing autism spectrum disorders. Am J Psychiatry 169:551–553.

Sundaram SK, Kumar A, Makki MI, Behen ME, Chugani HT, Chugani DC (2008): Diffusion tensor imaging of frontal lobe in autism spectrum disorder. Cereb Cortex 18:2659–2665.

Travers BG, Adluru N, Ennis C, Tromp DPM, Destiche D, Doran S, Bigler ED, Lange N, Lainhart JE, Alexander AL (2012): Diffusion tensor imaging in autism spectrum disorder: A review. Autism Res 5:289–313.

Wakana S, Caprihan A, Panzenboeck MM, Fallon JH, Perry M, Gollub RL, Hua K, Zhang J, Jiang H, Dubey P, Blitz A, van Zijl P, Mori S (2007): Reproducibility of quantitative tractography methods applied to cerebral white matter. Neuroimage 36: 630–644.

Wakana S, Jiang H, Nagae-Poetscher LM, van Zijl PC, Mori S (2004): Fiber tract-based atlas of human white matter anatomy. Radiology 230:77–87.

Walker L, Gozzi M, Lenroot R, Thurm A, Behseta B, Swedo S, Pierpaoli C (2012): Diffusion tensor imaging in young children with autism: biological effects and potential confounds. Biol Psychiatry 72:1043–1051.

Weinstein M, Ben-Sira L, Levy Y, Zachor DA, Ben Itzhak E, Artzi M, Tarrasch R, Eksteine PM, Hendler T, Ben Bashat D (2011): Abnormal white matter integrity in young children with autism. Hum Brain Mapp 32:534–543.

Wheeler-Kingshott CA, Cercignani M (2009): About 'axial' and 'radial' diffusivities. Magnet Reson Med. 61:1255–1260.

Wolff JJ, Gu H, Gerig G, Elison JT, Styner M, Gouttard S, Botteron KN, Dager SR, Dawson G, Estes AM, Evans AC, Hazlett HC, Kostopoulos P, McKinstry RC, Paterson SJ, Schultz RT, Zwaigenbaum L, Piven J, Network I (2012): Differences in white matter fiber tract development present from 6 to 24 months in infants with autism. Am J Psychiatry 169:589–600.

Woods RP, Grafton ST, Holmes CJ, Cherry SR, Mazziotta JC (1998): Automated image registration: I. General methods and intrasubject, intramodality validation. J Comput Assist Tomogr 22:139–152.

Zhao X, Leotta A, Kustanovich V, Lajonchere C, Geschwind DH, Law K, Law P, Qiu S, Lord C, Sebat J, Ye K, Wigler M (2007): A unified genetic theory for sporadic and inherited autism. Proc Natl Acad Sci USA 104:12831–12836.